KYBERNETIKA — VOLUME *58* (2022), NUMBER 2, PAGES 218–236

COORDINATION CONTROL AND ANALYSIS OF TCSC DEVICES TO PROTECT ELECTRICAL POWER SYSTEMS AGAINST DISRUPTIVE DISTURBANCES

Zhaoxu Wang, Chao Zhai, Hehong Zhang, Gaoxi Xiao, Guanghou Chen and Yulin Xu

In this work, we study coordination control and effective deployment of thyristor-controlled series compensation (TCSC) to protect power grids against disruptive disturbances. The power grid consists of flexible alternate current transmission systems (FACTS) devices for regulating power flow, phasor measurement units (PMUs) for detecting system states, and control station for generating the regulation signals. We propose a novel coordination control approach of TCSC devices to change branch impedance and regulate the power flow against unexpected disturbances on buses or branches. More significantly, a numerical method is developed to estimate a gradient vector for generating regulation signals of TCSC devices and reducing computational costs. To describe the degree of power system stress, a performance index is designed based on the error between the desired power flow and actual values. Moreover, technical analysis is presented to ensure the convergence of the proposed coordination control algorithm. Numerical simulations are implemented to substantiate that the coordination control approach can effectively alleviate the stress caused by contingencies on IEEE 24 bus system, as compared to the classic PID control. It is also demonstrated that the deployment of TCSCs can alleviate the system stress greatly by considering both impedance magnitude and active power on branches.

Keywords: coordination control, thyristor-controlled series compensation(TCSC), power systems, disruptive disturbances

LIST OF SYMBOLS AND ABBREVIATIONS

Constants

c: a small constant between 0 and 1
C_P, C_I, C_D: the parameters of PID controller
k: the update times of S_k
m, n: the total buses and branches of a power grid
T: the number of time steps in the interval
X_L: the reactance of transmission line between Bus i and Bus j
$\underline{Z}_i$, $\overline{Z}_i$: the lower and upper bound of Z_i
σ_i: the desired power flow of Branch i, $(i \in 1, \ldots, n)$

DOI: 10.14736/kyb-2022-2-0218

ϵ: a small constant
λ: a small perturbation

Variables

$H(\mathbf{Z})$: the objective function value of optimization problem
$H(\mathbf{Z}^*)$: the minimum value of optimization problem
$H_i(\mathbf{Z})$: the value of $H(\mathbf{Z})$ at the ith step
$J_{j,i}(\mathbf{Z})$: the element of $J(\mathbf{Z})$, $(i, j \in n)$
P_i: the inject active power of Bus i
$P_{e,j}(\mathbf{Z})$: the real time power flow of Branch j
$P^R_{e,j}(\mathbf{Z})$, $P^I_{e,j}(\mathbf{Z})$: the real and imaginary part of $P_{e,j}(\mathbf{Z})$
S_k: performance index
t: derivation time
V_i, V_j: the voltage of Bus i and Bus j, respectively
X_{TCSC}: reactance of TCSC
Z_i: the real time impedance of Branch i
θ_i, θ_j: the voltage phase angle of Bus i and Bus j, respectively
$\kappa_l(\mathbf{Z})$: the element of $\boldsymbol{\kappa}(\mathbf{Z})$, $(l \in 1, \ldots, 2n)$
μ, ς: the mean value and standard deviation of Gaussian noise disturbance

Vectors and matrixes

$\mathbf{e}_i$: unit vector
$\mathbf{I}$: the vector of bus current
$J(\mathbf{Z})$: the Jacobian matrix
$\mathbf{P}_b$: the power flow vector of buses
$\mathbf{P}_e$, $\mathbf{P}_e(\mathbf{Z})$: actual power flow of branches
$\mathbf{P}^R_e$, $\mathbf{P}^I_e$: the real and imaginary part of $\mathbf{P}_e$, respectively
$\Delta\mathbf{P}_e$: the error between $\mathbf{P}_e$ and the desired power flow σ
$\mathbf{V}$: the vector of bus voltage
$\mathbf{U}$: control input of designed coordination controller
$\mathbf{U}_R$, $\mathbf{U}_I$: the real and imaginary part of $\mathbf{U}$, respectively
$V(\mathbf{Z})$: the Lyapunov function candidate
$\mathbf{Z}$: the vector of branch impedance
$\mathbf{Z}^R$, $\mathbf{Z}^I$: the real and imaginary part of $\mathbf{Z}$, respectively
σ: the desired power flow vector of branches
σ^R, σ^I: the real and imaginary part of σ, respectively
$\boldsymbol{\kappa}(\mathbf{Z})$: the vector of tunable parameters

List of abbreviations

CCA: Coordination Control Algorithm
FACTS: Flexible Alternate Current Transmission Systems
KKT: Karush–Kuhn–Tucker
JEA: Jacobian Estimation Algorithm
PMUs: Phasor Measurement Units
TCSC: Thyristor-Controlled Series Compensation

1. INTRODUCTION

In the last decades, power system blackouts have become an intractable issue for both power industries and governments all over the world. To deal with this issue, some researchers focus on seeking the strategy of terminating cascading outages in the initial phase [26, 27], some researches are devoted to study the influence of communication delay on fault propagation by regarding power gird as a multi-agent system [14, 21], while other scholars try to identify disruptive disturbances (i. e., triggering events) [22, 28]. Considering that lots of blackouts are initiated because of the overload precondition [31], it is indispensable to alleviate the system stresses caused by overloads, which helps to avoid the catastrophic consequences and prevent cascading failures.

To alleviate system stresses, FACTS devices are employed to ensure power oscillation damping and improve the transient stability [13]. By regulating the power flow, TCSC devices enables to achieve the reliable operation of power grids [9]. So far, lots of control strategies have been developed, which include intelligent algorithms [4, 5, 24], finite-time H_∞ control approach [6], adaptive neural network backstepping control [17] and so on. With the assistance of second-order cone programming and model linearization, [2] analyzes the role of TCSC in alleviating the system stress. Moreover, [11, 32] design robust and nonlinear controllers for TCSC devices. To improve the transient stability [16, 18], the focus of existing work is on how to design standalone TCSC controllers or coordinate TCSC with other FACTS, which actually ignores the coordination control of TCSC devices against disruptive disturbances.

In practice, it is worth to study the coordination between TCSC devices for jointly reducing or eliminating the stress of power grid caused by various contingencies, since multi-agent coordination control has already widely applied in various fields [15, 29]. By sharing the information with neighboring agents, coordination control enables agents to coordinate individual control actions and achieve the control goal in a coordination manner. By treating each TCSC device as a smart agent, coordination control of TCSC can be used to protect power grids in real time [5]. By eliminating the stress of power grids systematically, it helps to strengthen the capability of power grids against disruptive disturbances [30]. For this reason, a coordination control approach is developed in the present work to alleviate the system stress. The main contributions of this work are summarized below:

1. Propose a novel coordination control approach for TCSC devices to regulate branch impedance in a coordination manner.

2. Develop an efficient numerical algorithm for estimating the gradient vector with low computation costs.

3. Provide an effective deployment strategy of TCSC devices to reduce the number of TCSC without weakening control performance. The deployment of TCSC considers the ability of dealing with contingencies, which includes the stress caused by power flow congestion.

The remainder of this paper is arranged as follows. Problem formulation on the coordination control of TCSC devices is provided in Section 2. The novel control scheme

of TCSC is presented in Section 3. IEEE test systems are employed to validate the proposed approach in Section 4. The conclusion is drawn in Section 5.

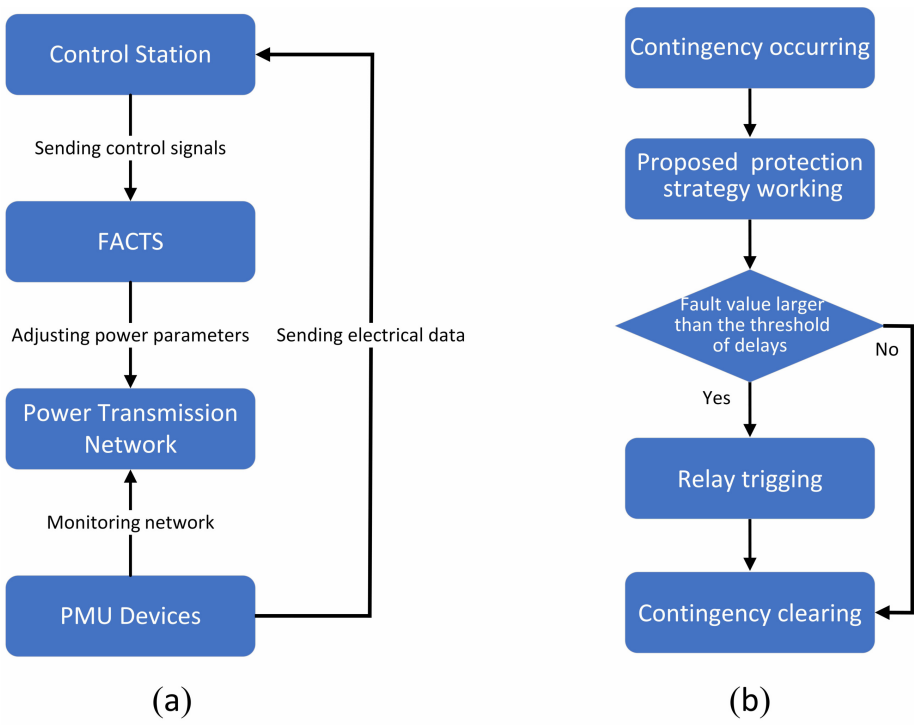

Fig. 1. (a) Smart power grids with PMU and FACTS. (b) Action sequence between the proposed protection strategy and delays.

2. PROBLEM FORMULATION

The smart power grid is comprised of transmission networks, phase measurement units, FACTS devices and control station (see Figure 1 (a)). More specifically, PMU is used to detect the state information of buses and send it to the control station in real time. The control station generates proper control signals to drive FACTS devices by using the state information. Finally, TCSC devices update the impedance of branches to regulate the power flow. The communication between TCSC, PMU and control station can be seen in Ref. [1, 25]. Synchronous optical networks (Sonet/SDH) and the asynchronous transfer mode (ATM) are the common communication protocols for exchanging data, and electrical utilities have their system management options for coping with problems. Figure 1 (b) shows the coordination relationship between the proposed protection strategy and delays. It is observed that the proposed protection strategy takes effect before the relays protective systems, and it has the complementary effect to the existing protection systems. Without loss of generality, consider a power grid with n branches

and m buses. When the power flow on the branch changes, TCSC devices adjust the branch impedance, so that the actual power flow $\mathbf{P}_e$ is restored to the desired values $\boldsymbol{\sigma} = (\sigma_1, \sigma_2, \ldots, \sigma_n) \in C^n$. To eliminate power system stresses, one needs to design a control input $\mathbf{U}$ for TCSC devices, and the optimization problem is formulated as follows.

$$\min_{\mathbf{U}} H(\mathbf{Z}) \tag{1}$$

with the objective function $H(\mathbf{Z}) = \|\mathbf{P}_e^R - \boldsymbol{\sigma}^R\|^2 + \epsilon\|\mathbf{P}_e^I - \boldsymbol{\sigma}^I\|^2$, where the vector of branch impedance is denoted by $\mathbf{Z}$ and $\epsilon \in [0, 1]$ is a tuning parameter. Note that $\mathbf{P}_e^R$ and $\mathbf{P}_e^I$ refer to the real part and imaginary part of $\mathbf{P}_e$, respectively. The superscripts R and I apply to other complex variables as well. To solve Problem (1), the Lyapunov function candidate $V(\mathbf{Z})$ is constructed below

$$V(\mathbf{Z}) = H(\mathbf{Z}) - H(\mathbf{Z}^*),$$

where $H(\mathbf{Z}^*)$ is the minimum value of Problem (1). Then the derivative of $V(\mathbf{Z})$ with respect to the time t gives

$$\frac{dV(\mathbf{Z})}{dt} = \frac{dH(\mathbf{Z})}{dt} = 2\left(\mathbf{P}_e^R - \boldsymbol{\sigma}^R\right)^T \frac{d\mathbf{P}_e^R}{dt} + 2\epsilon\left(\mathbf{P}_e^I - \boldsymbol{\sigma}^I\right)^T \frac{d\mathbf{P}_e^I}{dt} \tag{2}$$

with

$$\frac{d\mathbf{P}_e^R}{dt} = \frac{\partial \mathbf{P}_e^R}{\partial \mathbf{Z}^R} \cdot \frac{d\mathbf{Z}^R}{dt} + \frac{\partial \mathbf{P}_e^R}{\partial \mathbf{Z}^I} \cdot \frac{d\mathbf{Z}^I}{dt} \tag{3}$$

and

$$\frac{d\mathbf{P}_e^I}{dt} = \frac{\partial \mathbf{P}_e^I}{\partial \mathbf{Z}^R} \cdot \frac{d\mathbf{Z}^R}{dt} + \frac{\partial \mathbf{P}_e^I}{\partial \mathbf{Z}^I} \cdot \frac{d\mathbf{Z}^I}{dt}. \tag{4}$$

By substituting (3) and (4) into (2), one obtains

$$\begin{aligned}\frac{dV(\mathbf{Z})}{dt} &= 2\left(\mathbf{P}_e^R - \boldsymbol{\sigma}^R\right)^T \frac{\partial \mathbf{P}_e^R}{\partial \mathbf{Z}^R} \cdot \frac{d\mathbf{Z}^R}{dt} + 2\epsilon\left(\mathbf{P}_e^I - \boldsymbol{\sigma}^I\right)^T \frac{\partial \mathbf{P}_e^I}{\partial \mathbf{Z}^R} \cdot \frac{d\mathbf{Z}^R}{dt} \\ &\quad + 2\left(\mathbf{P}_e^R - \boldsymbol{\sigma}^R\right)^T \frac{\partial \mathbf{P}_e^R}{\partial \mathbf{Z}^I} \cdot \frac{d\mathbf{Z}^I}{dt} + 2\epsilon\left(\mathbf{P}_e^I - \boldsymbol{\sigma}^I\right)^T \frac{\partial \mathbf{P}_e^I}{\partial \mathbf{Z}^I} \cdot \frac{d\mathbf{Z}^I}{dt} \\ &= 2\begin{bmatrix} \mathbf{P}_e^R - \boldsymbol{\sigma}^R \\ \epsilon(\mathbf{P}_e^I - \boldsymbol{\sigma}^I) \end{bmatrix}^T J(\mathbf{Z}) \begin{bmatrix} \frac{d\mathbf{Z}^R}{dt} \\ \frac{d\mathbf{Z}^I}{dt} \end{bmatrix}.\end{aligned} \tag{5}$$

The Jacobian matrix $J(\mathbf{Z})$ in (5) is described by

$$J(\mathbf{Z}) = \begin{bmatrix} \frac{\partial \mathbf{P}_e^R}{\partial \mathbf{Z}^R} & \frac{\partial \mathbf{P}_e^R}{\partial \mathbf{Z}^I} \\ \frac{\partial \mathbf{P}_e^I}{\partial \mathbf{Z}^R} & \frac{\partial \mathbf{P}_e^I}{\partial \mathbf{Z}^I} \end{bmatrix} = (J_{i,j}(\mathbf{Z})) \in R^{2n \times 2n}. \tag{6}$$

The control input $\mathbf{U}$ is designed as

$$\mathbf{U} = \begin{bmatrix} \mathbf{U}_R \\ \mathbf{U}_I \end{bmatrix} = \begin{bmatrix} \frac{d\mathbf{Z}^R}{dt} \\ \frac{d\mathbf{Z}^I}{dt} \end{bmatrix}. \tag{7}$$

Because of the complexity of system model, it is not easy to directly obtain the accurate value of $J(\mathbf{Z})$. As a result, a numerical approach is proposed to estimate $J(\mathbf{Z})$. Moreover, this work does not convert the minimization Problem (1) into KKT condition, but directly design a coordination control method to minimize the value of $H(\mathbf{Z})$. The convergence of objective function $H(\mathbf{Z})$ is guaranteed by CCA, instead of KKT condition. Figure 2 shows the simplified control flow chart, specifically, PMUs

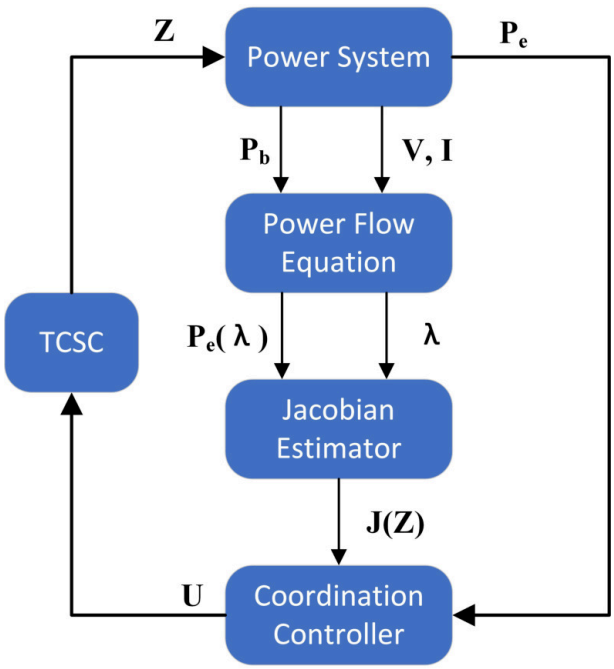

Fig. 2. Regulation signals in smart power grids equipped with TCSC devices.

collect time series of $\mathbf{P}_b$, $\mathbf{V}$ and $\mathbf{I}$. Then by injecting a small disturbance λ on the branch, the Jacobian matrix can be estimated based on power flow equation described in appendix. Finally the controller generates command signals for TCSC devices to regulate the power flow according to the designed control law, and the optimization goal is thus realized. For TCSC, it is general acknowledged that the TCSC device consists of two main control blocks, and the function of external control block is to improve the transmission capacity or stability of power grid [23]. According to different control objectives, external control can be designed using different methods. The traditional PI controller is a slow automatic control for power flow regulation [12], and the coordination control proposed in the present work can be regarded as a type of external control. The function of internal control block is to provide appropriate gate drive signals for thyristors to generate compensation reactance. The relationship between TCSC impedance and power flow is given in Appendix 6.1.

Remark 2.1. The goal of this work is to propose a novel coordination control method to regulate the impedance of branch by TCSC devices so as to alleviate the system stress. In fact, the proposed method is universal. It not only can be applied to TCSC devices, but also to other FACTS devices.

Remark 2.2. As presented in Appendix 6.2, the generic TCSC model aims to influence the branch power flow by changing the reactance. For the control strategy and algorithm designed in this work, the control signal $\mathbf{U}_R$ only needs to be set to zero, and control algorithm convergence can still be guaranteed.

3. DESIGN OF COORDINATION CONTROLLER

This section focuses on the design of coordination control law and discusses how to calculate $J(\mathbf{Z})$.

3.1. Generation of feedback control signals

The coordination control law for TCSC devices is given by

$$\mathbf{U} = -\boldsymbol{\kappa}(\mathbf{Z}) \circ J(\mathbf{Z})^T \begin{bmatrix} \mathbf{P}_e^R - \boldsymbol{\sigma}^R \\ \epsilon(\mathbf{P}_e^I - \boldsymbol{\sigma}^I) \end{bmatrix}, \tag{8}$$

where $\circ$ is the Hadamard product. Each element in $\boldsymbol{\kappa}(\mathbf{Z}) = (\kappa_1(\mathbf{Z}), \kappa_2(\mathbf{Z}), \ldots, \kappa_{2n}(\mathbf{Z}))^T$ is designed as

$$\kappa_i(\mathbf{Z}) = \begin{cases} c, & Z_i \in [\underline{Z}_i, \overline{Z}_i]; \\ 0, & \text{otherwise}, \end{cases}$$

with the constant $c > 0$ and the upper limit $\overline{Z}_i$ and lower limit $\underline{Z}_i$. The Coordination Controller (8) is composed of three terms: $\boldsymbol{\kappa}(\mathbf{Z})$, $J(\mathbf{Z})$ and the error vector

$$\Delta\mathbf{P}_e = \begin{bmatrix} \mathbf{P}_e^R - \boldsymbol{\sigma}^R \\ \epsilon(\mathbf{P}_e^I - \boldsymbol{\sigma}^I) \end{bmatrix}.$$

Specifically, $\boldsymbol{\kappa}(\mathbf{Z})$ allows to adjust the branch impedance in the given interval with upper and lower bounds. $J(\mathbf{Z})$ indicates the incremental direction of objective function with respect to branch impedance. $\Delta\mathbf{P}_e$ can be obtained by comparing the desired values with the actual ones.

Proposition 3.1. The Control Input (8) for TCSC devices can guarantee the convergence of $H(\mathbf{Z})$.

Proof. Note that both $\mathbf{Z}^R$ and $\mathbf{Z}^I$ are adjusted according to (8). By substituting (7) into (5) , one obtains

$$\frac{dV(\mathbf{Z})}{dt} = 2 \begin{bmatrix} \mathbf{P}_e^R - \boldsymbol{\sigma}^R \\ \epsilon(\mathbf{P}_e^I - \boldsymbol{\sigma}^I) \end{bmatrix}^T J(\mathbf{Z}) \begin{bmatrix} \mathbf{U}_R \\ \mathbf{U}_I \end{bmatrix}. \tag{9}$$

By substituting (8) into (9), one has

$$\frac{dV(\mathbf{Z})}{dt} = -2\begin{bmatrix} \mathbf{P}_e^R - \boldsymbol{\sigma}^R \\ \epsilon(\mathbf{P}_e^I - \boldsymbol{\sigma}^I) \end{bmatrix}^T J(\mathbf{Z}) \cdot \boldsymbol{\kappa}(\mathbf{Z}) \circ J(\mathbf{Z})^T \begin{bmatrix} \mathbf{P}_e^R - \boldsymbol{\sigma}^R \\ \epsilon(\mathbf{P}_e^I - \boldsymbol{\sigma}^I) \end{bmatrix}$$
$$= -2\left\| \bar{\boldsymbol{\kappa}}(\mathbf{Z}) \circ J(\mathbf{Z})^T \begin{bmatrix} \mathbf{P}_e^R - \boldsymbol{\sigma}^R \\ \epsilon(\mathbf{P}_e^I - \boldsymbol{\sigma}^I) \end{bmatrix} \right\|^2 \leq 0$$

where $\bar{\boldsymbol{\kappa}}(\mathbf{Z}) = (\sqrt{\kappa_1(\mathbf{Z})}, \sqrt{\kappa_2(\mathbf{Z})}, \ldots, \sqrt{\kappa_{2n}(\mathbf{Z})})^T$. This indicates that the objective function decreases monotonously as $t \to +\infty$. Thus, $H(\mathbf{Z})$ is convergent because of $H(\mathbf{Z}) \geq 0$. □

3.2. Construction of Jacobian estimator

The implementation of the proposed CCA calls for the estimation of $J(\mathbf{Z})$. In [8], the linear total least-square is employed to calculate $J(\mathbf{Z})$. Although the approximations and relaxations exist in the modeling of relevant problems, the process is still complicated and requires a large amount of calculations. Thus, it is indispensable to come up with a numerical method to estimate $J(\mathbf{Z})$ with low computation burdens. The approximation of Jacobian matrix includes four steps. In the 1st step, $\mathbf{P}_e(\mathbf{Z})$ is calculated. Then a small disturbance λ is injected onto each branch, and the disturbed power flow $\mathbf{P}_e(\mathbf{Z}^R + \lambda\mathbf{e}_i)$ is obtained, where $\mathbf{e}_i$ denotes the unit vector with the ith entry being 1. In light of Taylor's theorem, $P_{e,j}^R(\mathbf{Z}^R + \lambda\mathbf{e}_i)$ and $P_{e,j}^I(\mathbf{Z}^R + \lambda\mathbf{e}_i)$ can be rewritten as

$$P_{e,j}^R(\mathbf{Z}^R + \lambda\mathbf{e}_i) = P_{e,j}^R(\mathbf{Z}) + \lambda\frac{\partial P_{e,j}^R}{\partial \mathbf{Z}^R}\mathbf{e}_i + O(\lambda) = P_{e,j}^R(\mathbf{Z}) + \lambda J_{j,i}(\mathbf{Z}) + O(\lambda)$$

and

$$P_{e,j}^I(\mathbf{Z}^R + \lambda\mathbf{e}_i) = P_{e,j}^I(\mathbf{Z}) + \lambda\frac{\partial P_{e,j}^I}{\partial \mathbf{Z}^R}\mathbf{e}_i + O(\lambda) = P_{e,j}^I(\mathbf{Z}) + \lambda J_{j+n,i}(\mathbf{Z}) + O(\lambda),$$

respectively. After removing $O(\lambda)$, elements in the ith column of $J(\mathbf{Z})$ are given by

$$J_{j,i}(\mathbf{Z}) \approx \frac{P_{e,j}^R(\mathbf{Z}^R + \lambda\mathbf{e}_i) - P_{e,j}^R(\mathbf{Z})}{\lambda}, \tag{10}$$

$$J_{j+n,i}(\mathbf{Z}) \approx \frac{P_{e,j}^I(\mathbf{Z}^R + \lambda\mathbf{e}_i) - P_{e,j}^I(\mathbf{Z})}{\lambda}. \tag{11}$$

Finally, $Re(Z)$ is restored. Similarly, elements in the $(i+n)$th column of $J(\mathbf{Z})$ are presented as

$$J_{j,i+n}(\mathbf{Z}) \approx \frac{P_{e,j}^R(\mathbf{Z}^I + \lambda\mathbf{e}_i) - P_{e,j}^R(\mathbf{Z})}{\lambda}, \tag{12}$$

$$J_{j+n,i+n}(\mathbf{Z}) \approx \frac{P_{e,j}^I(\mathbf{Z}^I + \lambda\mathbf{e}_i) - P_{e,j}^I(\mathbf{Z})}{\lambda}. \tag{13}$$

Algorithm 1 summaries how to estimate $J(\mathbf{Z})$ in the numerical method. To alleviate computation burdens, a performance index is designed as $S_k = \max_{i\in I(k)} H_i(\mathbf{Z})$, where $I(k) = [(k-1)T + 1, kT]$, $\forall k \in \mathbb{Z}^+$, and $H_i(\mathbf{Z})$ denotes the value of $H(\mathbf{Z})$ at the ith step.

Algorithm 1 Jacobian Estimation Algorithm.

Input: λ and P_b
Output: $J(Z)$

Set λ and detect P_b
Compute $P_e(Z)$
for $i = 1$ to n do
  $\mathtt{Re}(Z) = \mathtt{Re}(Z) + \lambda e_i$
  Compute $P_e(Z^R + \lambda e_i)$
  Estimate $J_{j,i}(Z)$ with (10) and (11)
  $\mathtt{Re}(Z) = \mathtt{Re}(Z) - \lambda e_i$
  $\mathtt{Im}(Z) = \mathtt{Im}(Z) + \lambda e_i$
  Compute $P_e(Z^I + \lambda e_i)$
  Estimate $J_{j,i+n}(Z)$ with (12) and (13)
  $\mathtt{Im}(Z) = \mathtt{Im}(Z) - \lambda e_i$
end for

Algorithm 2 Coordination Control Algorithm.

Input: $s = 0$, $k = 0$, $T = 100$ and $S_0 = H_0(\mathbf{Z})$
Output: Z and P_e

while $(H_s(\mathbf{Z}) \neq 0)$
  Detect P_e
  if $(\mathtt{mod}(s, T) = 0)$
    Update $k = k + 1$
    Compute S_k
    if $(S_k \geq S_{k-1})$ or $(s = 0)$
      $S_k \leftarrow S_{k-1}$
      Detect P_b, V and I
      Run the JEA for $J(Z)$
    end if
  end if
  Update Z with (8)
  Update $s = s + 1$
  Compute $H_s(\mathbf{Z})$
end while

The implementation of proposed coordination controller is described in Algorithm 2, and it allows to decrease the performance index S_k.

Proposition 3.2. CCA for TCSC devices in Algorithm 2 guarantees the monotonous convergence of S_k.

Proof. CCA enables to produce a sequence $\{S_k\}_{k=1}^{\infty}$. It follows from $S_{k+1} \leq S_k$ and $S_k \geq 0$, $\forall k \in \mathbb{Z}^+$ that S_k converges to a constant value $\inf_{k\in\mathbb{Z}^+} S_k$ monotonously as k approaches the positive infinity. □

Remark 3.1. The final value of S_k is an unknown constant related to the disturbances on power system. When the disturbances are small, S_k converges to zero. Otherwise, the disturbances are large and the proposed control strategy cannot eliminate them, S_k will converge to a constant.

4. NUMERICAL SIMULATIONS

Extensive simulation results are presented to demonstrate the performance of the proposed control approach, and the locations of TCSCs and PMUs are shown in Figure 3. Some key parameters are given below: $c = 0.02$, $\epsilon = 0.2$, $\lambda = 10^{-6}$ and $T = 100$. The parameters of PID control are presented as $C_P = 2 \times 10^{-5}$, $C_I = 10^{-2}$, $C_D = 3 \times 10^{-6}$. Euler method is employed to implement the control algorithm with the step size of 0.01 and the total time steps 10^4. In addition, the adjustment range of branch impedance is 0.8 to 1.7 times larger than the magnitude of the steady-state value. Per unit systems are employed using base value of 100 MVA.

Next, simulation cases are evaluated to assess the performance of CCA. They include cases with disturbances on single or multiple branches and the effects of TCSC deployment on system resilience by using the proposed CCA.

4.1. Disturbances on single or multiple branches

This subsection will analyze how to use the CCA to relieve the stress of power system caused by disruptive disturbances. Two types of emergencies are tested, with change of branch impedance on one transmission line and changes of branch impedance on multiple transmission lines, respectively. Table 1 shows the branch data selected according to power system data and network topology. Further details of those two contingencies are summarized in Table 2. Specifically, the first column lists the test ID, the second column presents the branch ID where disruptive disturbances are added, the third column provides the value of branch impedance after contingencies, and the last column provides the disruption caused by faults to the whole buses. For simplicity, it is assumed that the injected bus power is subject to the disturbances, which satisfy the normal distribution with a mean value of $\mu = 0$ and standard deviation of $\varsigma = 0.1$ in Test 1. One defines the disturbances in Test 1 as the unit value, and the disturbances in subsequent tests are compounded by the unit value. The desired power flow σ is specified as power flow in the normal condition before the initial contingency.

Branch ID	From Bus	To Bus	R(pu)	X(pu)
5	2	6	0.0492	0.1920
6	3	9	0.0308	0.1190
29	16	19	0.0030	0.0231
36	20	23	0.0028	0.0216

Tab. 1. Branch parameters.

Test sequence	Branch ID	Fault values of branch reactance X(pu)	Disruption [Gaussian noise]
1	5	0.096	1
2	5,6,29,36	0.096,0.0595,0.0116,0.0108	1.5

Tab. 2. The location and parameters of contingencies.

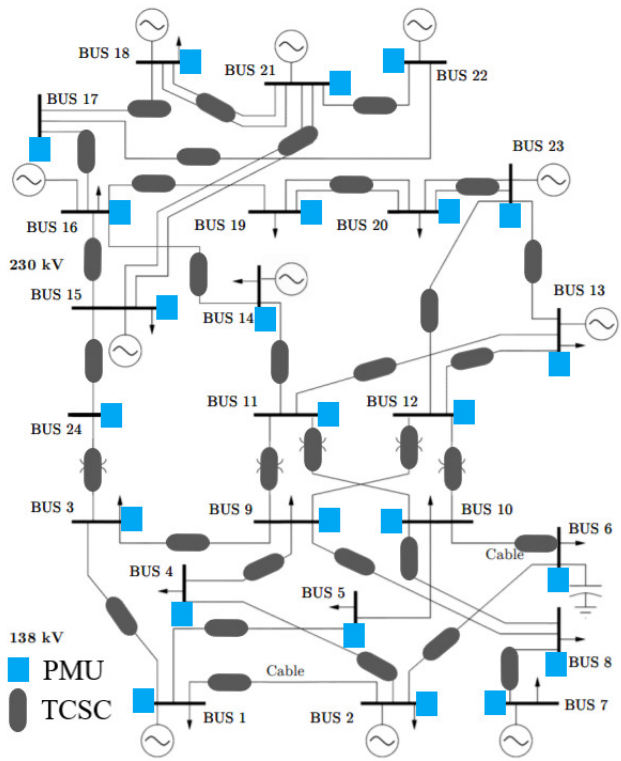

Fig. 3. IEEE 24 bus system equipped with TCSC devices and PMUs.

Figure 4 (a)–(b) demonstrates that the objective function $H(\mathbf{Z})$ monotonously decreases from the initial value to the final value in each test. Specially, $H(\mathbf{Z})$ decreases rapidly from 0.0926 to 0.0075 in Test 1 and from 0.3577 to 0.0968 in Test 2. It is observed that $H(\mathbf{Z})$ gradually converges to small positive values in those two tests, which indicates the effectiveness of coordination control between TCSCs to relieve the stress of power system. The blue trajectories in Figure 4 (c)–(d) show the monotonous decrease of S_k from the initial value to the final value, which partially confirms the conclusion of Proposition 3.2. The total number of k is 100 since S_k is computed for every $T = 100$

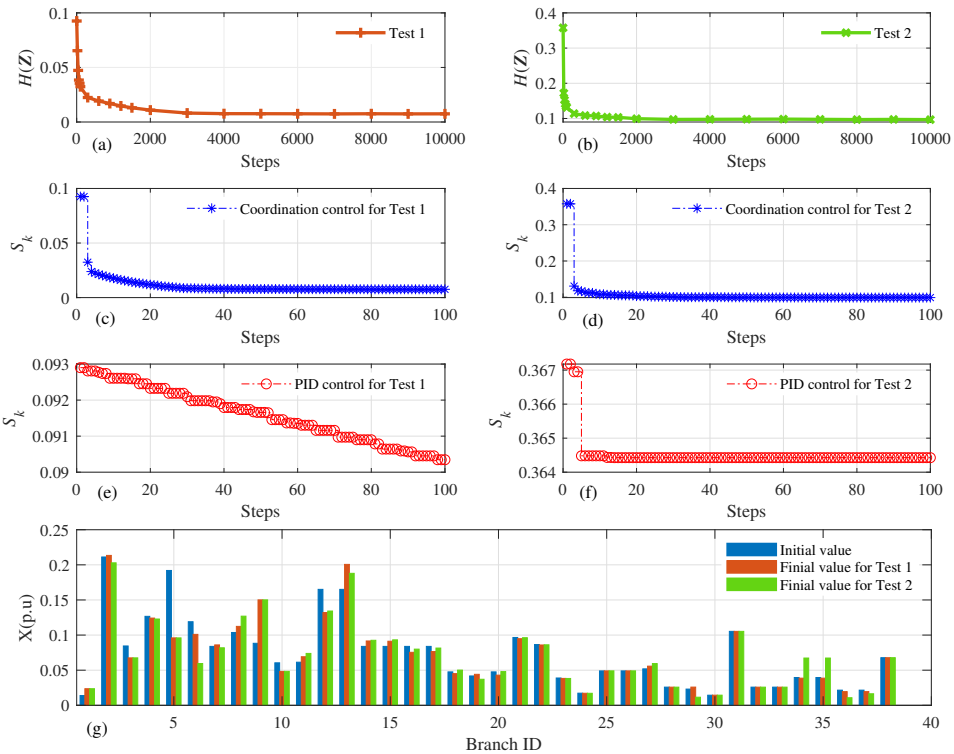

Fig. 4. (a)-(b): The trajectories of the objective function $H(\mathbf{Z})$ in different tests. (c)-(d): The trajectories of S_k in two tests by using coordination control algorithm. (e)-(f): the trajectories of S_k in three tests by using PID control algorithm. (g): The initial value and final value of branch reactance in different tests.

steps with the total steps of 10^4. In addition, the Jacobian matrix $J(\mathbf{Z})$ is updated 30 times in the simulation. By contrast, the red trajectories in Figure 4 (e)–(f) display the evolution of S_k with the PID control for each TCSC. It is obvious that S_k decreases rapidly by using coordination control scheme, while S_k only changes slightly with the PID control algorithm. Figure 4 (g) presents the comparison of branch reactance at the initial step and the final step in two tests by using the CCA. By observing the final values of the three tests, one can see that changes of branch impedance are different in each test, which means that changing branch impedance by the CCA is feasible. It is also observed that adjusting the impedance values of some TCSCs can effectively relieve the stress, one further looks into the effects of the number and deployment of TCSC on the effectiveness of CCA.

Finally, the stability of CCA is evaluated by changing the mean value and standard

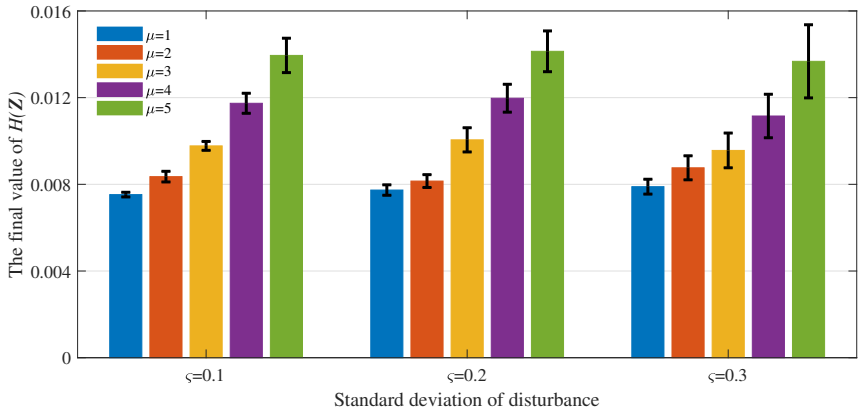

Fig. 5. The changes of the average value of $H(\mathbf{Z})$ in the final step with the increase of mean value μ and standard deviation ς of Gaussian noise disturbance.

deviation of the disturbances based on Test 1. In each group, simulations are carried out for 10 times, and the average values of the objective function $H(\mathbf{Z})$ in the final step are analyzed. Figure 5 shows the mean value and standard deviation of $H(\mathbf{Z})$ in the final step with the intensity of disturbances. Again, it is shown that the proposed CCA can effectively eliminate the stress of power system.

4.2. Effects of TCSC deployment on system resilience

In order to enhance power system resilience, measures can be taken in three phases [3] and [20]: identification and prediction before disaster, fast response when disaster occurs and system recovery after disaster. This work focuses on the ability of a power system to recover quickly after suffering from disruptive disturbances. The goal is to minimize the influence of disturbance as soon as possible via coordination control of TCSCs. In practice, TCSC may not be installed on all branches due to the high cost, it is necessary to investigate the strategy of reducing the number of TCSC and deployment of TCSC without impairing the control performance and the resilience of power systems. The existing literature only considered power flow congestion when studying the optimal deployment of TCSCs. In [10], an evolutionary NSGA-II algorithm is adopted to determine the optimal deployment of TCSC, which aims to maximise the available transmission capacity of branches. However, the implementation of the control strategy is based on DC power flow, it may deviate from the actual operation of power system. Ref. [19] utilizes the multi-objective genetic algorithm to determine the optimal locations of TCSCs, and the total power loss is reduced based on the optimal deployment of TCSCs. This paper considers the deployment of TCSCs from the perspective of reducing power system stress, which also includes power flow congestion problem.

According to the active power on branches, one considers TCSC installation at three different levels, where TCSCs are only installed on branches with active power more

Test sequence	Branch ID that installed TCSC	Total TCSC number	The level that active power on branches
Test 1	7,15-17,19,21-23, 25-28,30,31,38	15	More than 1.2 pu
Test 2	7,16,17,19,21-23, 25-28,30,38	13	More than 1.5 pu
Test 3	7,21-23,25-28, 30	9	More than 1.8 pu
Test 4	7,21-23,25-28, 30,38	10	-

Tab. 3. The location of branches that installed with TCSC devices.

Test sequence	1	2	3	4
Total TCSC number	14	11	8	9
Average value of $H(\mathbf{Z})$ in the final step	0.0029	0.0029	0.1341	0.0029

Tab. 4. The relationship between the average value of $H(\mathbf{Z})$ in the final step for ten times and the number of TCSC.

than 1.2 pu (Test 1), on branches with active power more than 1.5 pu (Test 2), and on branches with active power more than 1.8 pu (Test 3), respectively. The location of TCSCs is shown in Table 3. In Test 4, another TCSC is installed on Branch 38 connecting Bus 21 and Bus 22 in addition to the deployment in Test 3. The initial contingency is added on the Branch 31, which set as the branch reactance to 1.5 times of normal value. The injected bus power is subject to the disturbances, which satisfy the unit value(defined in 4.1). Table 4 shows the average value of $H(\mathbf{Z})$ in the final step for 10 simulations in each test. When the contingency occurs on Branch 31, $H(\mathbf{Z})$ in Test 1 and Test 2 decreases rapidly from 0.2582 to 0.0029, respectively, where the number of TCSC are 15 in Test 1 and 13 in Test 2. This confirms the fact that it is feasible to reduce the number of TCSC according to active power. In Test 3, the number of TCSCs is reduced to 9, where TCSCs are only installed on branches with higher power flow. It can be seen that $H(\mathbf{Z})$ decreases from 0.2582 to 0.1341 and CAA cannot effectively alleviate the stress of power grid.

In order to figure out why the final value of $H(\mathbf{Z})$ suddenly increases in Test 3, the impedance changes on all branches in Test 1 to Test 3 are analyzed, as presented in Figure 6. It is noted that the reactance of Branch 38 plays a major role in Test 1 and Test 2. Since the active power on Branch 38 is 1.56pu, which is lower than 1.8pu and TCSC is not installed on Branch 38 in Test 3 when the contingency occurrs, it is not feasible to relieve the stress caused by disturbance by adjusting the impedance value of the other branches. To test whether the TCSC device installed on Branch 38 indeed

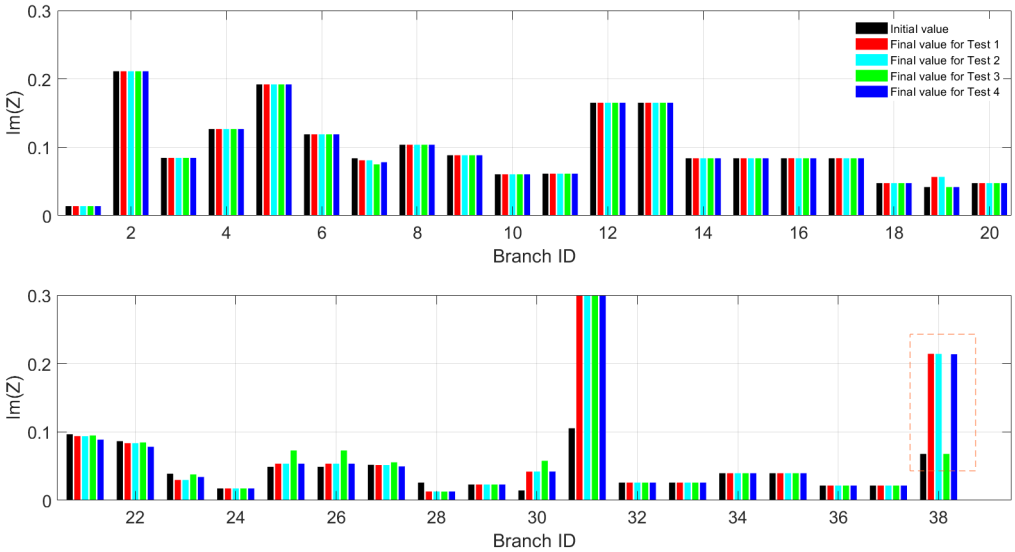

Fig. 6. Distribution of branch reactance at the initial step and the final step of the numerical simulations.

plays a critical role, one lets TCSC be reinstalled on Branch 38. This leads to Test 4. Simulation results show that $H(\mathbf{Z})$ converges rapidly and returns to the same level as that in Test 1 and Test 2. Note that the number of TCSCs installed on branch in Test 4 is still less than those in Test 1 and Test 2.

According to simulation results, it is suggested that the effective deployment of TCSCs does not merely depend on the branch capacity. In other words, it might not be feasible to effectively relieve the stress of power grid by only installing TCSC on the transmission lines with relatively large transmission capacity. It is observed that the impedance of a branch with higher power flow is relatively smaller, while the power flow on a branch with large impedance is relatively smaller. If TCSCs are installed on branches with higher power flow, the adjustable range of TCSC is relatively small, which may result in the failure of relieving stresses by adjusting the TCSC impedance. Therefore, it is desirable to install TCSCs on the branches with relatively large impedance in order to expand their regulation range with the coordination control algorithm, which helps to improve the stability of the entire power system greatly.

5. CONCLUSION AND FUTURE WORK

A novel coordination control algorithm was developed to alleviate the system stress by regulating power flow with the assistance of TCSC devices. It also provided the design method of the coordination controller and proved the convergence of the proposed control algorithm. Simulation results for different types of disturbances indicate the excellent stability of the proposed coordination control approach, as compared to the

traditional control methods. Finally, simulation results also demonstrated that the effective deployment of TCSCs is closely relevant to the magnitude of branch impedance, which is a novel approach to reduce the number of TCSCs.

Future work may include optimal deployment of limited TCSC agents on the entire power network by using distributed control method [7], and the estimation of Jacobian elements by analyzing the real PMU data without disturbing the branch impedance. Furthermore, it is our plan to design the multi-states control strategy for enhancing the system resilience with considering the existing delay protection systems.

6. APPENDIX

6.1. AC power flow equation

The follows power flow equations can be used for calculating injecting power of Bus i.

$$\begin{aligned} P_{b,i}^{R} &= \sum_{j=1}^{m} |V_i|\,|V_j|\,(G_{i,j}\cos\theta_{i,j} + B_{i,j}\sin\theta_{ij}) \\ P_{b,i}^{I} &= \sum_{j=1}^{m} |V_i|\,|V_j|\,(G_{i,j}\sin\theta_{i,j} - B_{i,j}\cos\theta_{ij})\,, \end{aligned} \tag{14}$$

where $Y = G_{i,j} + jB_{i,j}$ is the reciprocal of impedance $Z_{i,j}$, $\theta_{i,j}$ is the voltage phase angle of Branch i, j connecting Bus i and Bus j.

6.2. A general TCSC model

This subsection provides the relation between TCSC impedance and power flow on branches. Figure 7 shows the TCSC model of branch i, j connecting Bus i and Bus j, and the reactance of TCSC can be calculated with the power flow equations as follows:

$$\begin{aligned} P_{i,j} &= \frac{V_i V_j}{X_{i,j}}\sin\theta_{i,j} \\ Q_{i,j} &= \frac{1}{X_{i,j}}\left(V_i^2 - V_i V_j\cos\theta_{i,j}\right) \end{aligned} \tag{15}$$

with $X_{i,j} = X_{TCSC} + X_L$. X_{TCSC} and X_L represent the reactance of TCSC and transmission line between Bus i and Bus j, respectively.

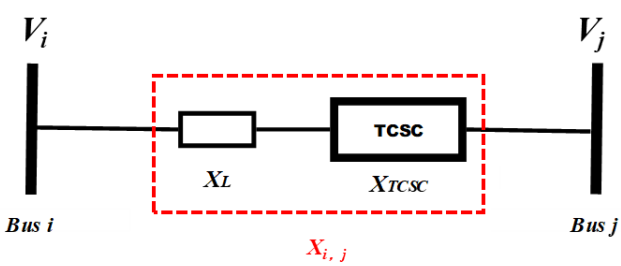

Fig. 7. TCSC model on a branch.

ACKNOWLEDGEMENT

This work is supported by the Fundamental Research Funds for the Central Universities, China University of Geosciences (Wuhan). It is partially supported by the Future Resilient Systems Programme (FRS-II) at the Singapore-ETH Centre (SEC), which is funded by the National Research Foundation of Singapore (NRF) under its Campus for Research Excellence and Technological Enterprise (CREATE) program. It is also supported by the National Natural Science Foundation of China (62003088) and the National Natural Science Foundation of Fujian Province (2021J02008).

(Received June 1, 2022)

REFERENCES

[1] M. Begovic, D. Novosel, D. Karlsson, C. Henvill, and G. Michel: Wide-area protection and emergency control. Proc. T. IEEE *93* (2005), 876–891. DOI:10.1109/JPROC.2005.847258

[2] R. Bi, T. Lin, R. Chen, J. Ye, X. Zhou, and X. Xu: Alleviation of post-contingency overloads by SOCP based corrective control considering TCSC and MTDC. IET Gener. Transmiss. Distr. *12* (2018), 2155–2164. DOI:10.1049/iet-gtd.2017.1393

[3] Z. Bie, Y. Lin, G. Li, and F. Li: Battling the extreme: A study on the power system resilience. Proc. T. IEEE *105* (2017), 1253–1566. DOI:10.1109/JPROC.2017.2679040

[4] S. Biswas and K. P. Nayak: A new approach for protecting TCSC compensated transmission lines connected to DFIG-based wind farm. IEEE Trans. Industr. Inform. *17* (2021), 5282–5291. DOI:10.1109/TII.2020.3029201

[5] S. Bruno, G. De, and M. La: Transmission grid control through TCSC dynamic series compensation. IEEE Trans. Power Syst. *31* (2016), 3202–3211. DOI:10.1109/TPWRS.2015.2479089

[6] L. Chang, Y. Liu, Y. Jing, X. Chen, and J. Qiu: Semi-globally practical finite-time H_∞ control of TCSC model of power systems based on dynamic surface control. IEEE Access. *8* (2020), 10061–10069. DOI:10.1109/ACCESS.2020.2964265

[7] Z. Chen and L. Shu: Distributed aggregative optimization with quantized communication. Kybernetika *58* (2022), 123–144. DOI:10.1155/2022/3436530

[8] Y. Chen, J. Wang, A. D. Domínguez-García, and P. W. Sauer: Measurement-based estimation of the power flow Jacobian matrix. IEEE Trans. Smart Grid *7* (2015), 2507–2515. DOI:10.1109/TSG.2015.2502484

[9] T. Duong, J. Yao, and V. Truong: A new method for secured optimal power flow under normal and network contingencies via optimal location of TCSC. Int. J. Electr. Power Energy Syst. *52* (2013), 68–80. DOI:10.1016/j.ijepes.2013.03.025

[10] V. Durković and A. Savić: ATC enhancement using TCSC device regarding uncertainty of realization one of two simultaneous transactions. Int. J. Electr Power Energy Syst. *115* (2020), 105497. DOI:10.1016/j.ijepes.2019.105497

[11] A. Halder, N. Pal, and D. Mondal: Transient stability analysis of a multimachine power system with TCSC controller – A zero dynamic design approach. Int. J. Electr Power Energy Syst. *97* (2018), 51–71. DOI:10.1016/j.ijepes.2017.10.030

[12] S. Hameed, B. Das, and V. Pant: A self-tuning fuzzy PI controller for TCSC to improve power system stability. Electr. Pow. Syst. Res. *78* (2008), 1726–1735. DOI:10.1016/j.epsr.2008.03.005

[13] R. Hemmati, H. Faraji, and Y. N. Beigvand: Multi objective control scheme on DFIG wind turbine integrated with energy storage system and FACTS devices: Steady-state and transient operation improvement. Int. J. Electr. Power Energy Syst. *135* (2022), 107519. DOI:10.1016/j.ijepes.2021.107519

[14] J. Hu: On Robust Consensus of Multi-Agent Systems with Communication Delays Volume. Kybernetika *45* (2009), 768–784.

[15] J. Hu, G. Chen, and H. Li: Distributed event-triggered tracking control of leader-follower multi-agent systems with communication delays. Kybernetika *47* (2011), 630–643.

[16] Y. Liu, Q. Wu, and X. Zhou: Coordinated switching controllers for transient stability of multi-machine power systems. IEEE Trans. Power Syst. *31* (2016), 3937–3949. DOI:10.1109/TPWRS.2015.2495159

[17] Y. Luo, S. Zhao, D. Yang, and H. Zhang: A new robust adaptive neural network backstepping control for single machine infinite power system with TCSC. IEEE/CAA J. Automat. Sinica *7* (2020), 48–56. DOI:10.1109/JAS.2019.1911798

[18] H. Kumar and P. Singh: Coordinated control of TCSC and UPFC to aid damping oscillations in the power system. Int. J. Electron. *106* (2019), 1938–1963. DOI:10.1080/00207217.2019.1636296

[19] T. Nguyen and F. Mohammadi: Optimal placement of TCSC for congestion management and power loss reduction using multi-objective genetic algorithm. Sustainability *12* (2020), 2813. DOI:10.3390/su12072813

[20] M. Panteli and P. Mancarella: The grid: Stronger, bigger, smarter?: Presenting a conceptual framework of power system resilience. IEEE Pow. Energy Mag. *13* (2015), 58–66. DOI:10.1109/MPE.2015.2397334

[21] T. Prakash, P. V. Singh, and S. R. Mohanty: A synchrophasor measurement based wide-area power system stabilizer design for inter-area oscillation damping considering variable time-delays. Int. J. Electr Power Energy Syst. *105* (2019), 131–141. DOI:10.1016/j.ijepes.2018.08.014

[22] R. Rocchetta and E. Patelli: Assessment of power grid vulnerabilities accounting for stochastic loads and model imprecision. Int. J. Electr. Power Energy Syst. *98* (2018), 219–232. DOI:10.1016/j.ijepes.2017.11.047

[23] A. Rosso, C. A. Canizares and V. M. Dona: A study of TCSC controller design for power system stability improvement. IEEE Trans. Power Syst. *18* (2003), 1487–1496. DOI:10.1109/TPWRS.2003.818703

[24] B. Shafik, H. Chen, I. Rashed, and A. Sehiemy: Adaptive multi objective parallel seeker optimization algorithm for incorporating TCSC devices into optimal power flow framework. IEEE Access. *7* (2019), 36934–36947. DOI:10.1109/ACCESS.2019.2905266

[25] V. Terzija, G. Valverde, D, Cai. P, Regulski, V. Madani, J. Fitch, S. Skok, M. Begovic, and A. Phadke: Wide-area monitoring, protection, and control of future electric power networks. Proc. T. IEEE *99* (2011), 80–93. DOI:10.1109/JPROC.2010.2060450

[26] J. Xu, R. Yao and F. Qiu: Mitigating cascading outages in severe weather using simulation-based optimization. IEEE Trans. Power Syst. *39* (2021), 204–213. DOI:10.1109/tpwrs.2020.3008428

[27] C. Zhai, G. Xiao, M. Meng, H. Zhang, and B. Li: Identification of catastrophic cascading failures in protected power grids using optimal control. J. Energ. Engrg. *147* (2021), 6020001. DOI:10.1061/(ASCE)EY.1943-7897.0000731

[28] C. Zhai, G. Xiao, H. Zhang, P. Wang, and T. Pan: Identifying disruptive contingencies for catastrophic cascading failures in power systems. Int. J. Electr. Power Energy Syst. *123* (2020), 106214. DOI:10.1016/j.ijepes.2020.106214

[29] C. Zhai and Y. Hong: Decentralized sweep coverage algorithm for multi-agent systems with workload uncertainties. Automatica *49* (2013), 2154–2159. DOI:10.1016/j.automatica.2013.03.017

[30] C. Zhai, G. Xiao, H. Zhang and T. Pan: Cooperative control of TCSC to relieve the stress of cyber-physical power system. In: International Conference on Control, Automation, Robotics and Vision 2018, pp. 4849–4854. DOI:10.1186/s13662-018-1910-6

[31] C. Zhai, H. Zhang, G. Xiao, and T. Pan: A model predictive approach to protect power systems against cascading blackouts. Int. J. Electr. Power Energy Syst. *113* (2019), 310–321. DOI:10.1016/j.ijepes.2019.05.029

[32] C. Zhang, X. Wang, Z. Ming, Z. Cai, and H. Linh: Enhanced nonlinear robust control for TCSC in power system. Math. Probl. Eng. *2018* (2018), 1416059. DOI:10.1155/2018/3495096

Zhaoxu Wang, School of Automation, China University of Geosciences, Wuhan 430074 China; Hubei Key Laboratory of Advanced Control and Intelligent Automation for Complex Systems; Engineering Research Center of Intelligent Technology for Geo-Exploration, Ministry of Education Wuhan 430074. P. R. China.
e-mail: wzx@cug.edu.cn

Chao Zhai, School of Automation, China University of Geosciences, Wuhan 430074 China; Hubei Key Laboratory of Advanced Control and Intelligent Automation for Complex Systems; Engineering Research Center of Intelligent Technology for Geo-Exploration, Ministry of Education Wuhan 430074. P. R. China.
e-mail: zhaichao@amss.ac.cn

Hehong Zhang, Corresponding author. College of Computer and Data Science, Fuzhou University, Fuzhou 350108. P. R. China.
e-mail: HZHANG030@e.ntu.edu.sg

Gaoxi Xiao, School of Electrical and Electronic Engineering, Nanyang Technological University, 50 Nanyang Avenue, Singapore 639798. Singapore.
e-mail: egxxiao@ntu.edu.sg

Guanghou Chen, Sanming City Construction and Development Group Co., Ltd.
e-mail: 498501396@qq.com

Yulin Xu, CYG SUNRI CO. LTD., Shenzhen 518057. P. R. China.
e-mail: xuyl@sznari.com